inbreeding coefficients (IBCs) revealed that only 0.5% of pairings resulted in individuals with an IBC greater than 0, and there was no evidence for between-year heterogeneity in IBCs (Kruskal–Wallis $H_{18} = 15.15$, $P = 0.65$; estimated using Pedigree Viewer, available from http:// www.personal.une.edu.au/~bkinghor/pedigree.htm). Changes in EBVs across generations can therefore be taken as evidence of a response to selection, or 'genetic trend'[27,28]. Genetic correlations were estimated from a multivariate animal model analysis of fledgling condition, life-span (LSP; in years) and lifetime reproductive success (LRS; defined as the number of offspring recruited into the breeding population). Genetic correlation analyses were necessarily restricted to individuals surviving to adulthood; area and year were included as random effects, and sex (known for individuals recaptured as adults) as a fixed effect.

Selection analyses

Estimates of survival selection on phenotypic and estimated breeding values of condition index were based on recapture data under the assumption that nestlings not returning to the study area in subsequent years had died. As many of the individuals recruit to the population at the age of two years, the survival analyses were restricted to the period of 1981–1998. Standardized directional (S) and quadratic (c^2) selection differentials were estimated by linear regression of relative fitness on standardized (zero mean, unit variance) phenotypic or breeding values of the condition index using standard methods[29]. Statistical significance of the selection differentials was estimated with logistic regression[29]. Associations between individual LSP or LRS and EBVs for condition were tested using GLMMs with negative binomial error structure, using the procedure IRREML in Genstat[30]. Nest of origin, year and area were included as random effects in the model, to account for repeated measures. The significance of the fixed effect of condition breeding value as a predictor of LSP or LRS was assessed by the Wald statistic, distributed as $\chi^2_{(1)}$ (ref. 30).

Received 26 February; accepted 14 May 2001.

1. Grant, P. R. & Grant, B. R. Predicting microevolutionary responses to directional selection on heritable variation. *Evolution* **49,** 241–251 (1995).
2. Reznick, D. N., Shaw, F. H., Rodd, F. H. & Shaw, R. G. Evaluation of the rate of evolution in a natural population of guppies. *Science* **275,** 1934–1937 (1997).
3. Price, T., Kirkpatrick, M. & Arnold, S. J. Directional selection and the evolution of breeding date in birds. *Science* **240,** 798–799 (1988).
4. Alatalo, R. V., Gustafsson, L. & Lundberg, A. Phenotypic selection on heritable size traits: environmental variance and genetic response. *Am. Nat.* **135,** 464–471 (1990).
5. Cooke, F., Taylor, P. D., Frances, C. M. & Rockwell, R. F. Directional selection and clutch size in birds. *Am. Nat.* **136,** 261–267 (1990).
6. Frank, S. A. & Slatkin, M. Fisher's fundamental theorem of natural selection. *Trends Ecol. Evol.* **7,** 92–95 (1992).
7. Lynch, M. & Walsh, B. *Genetics and Analysis of Quantitative Traits* (Sinauer, Sunderland, Massachusetts, 1998).
8. Roff, D. A. *Evolutionary Quantitative Genetics* (Chapman & Hall, New York, 1997).
9. Hochachka, W. & Smith, J. N. Determinants and consequences of nestling condition in song sparrows. *J. Anim. Ecol.* **60,** 995–1008 (1991).
10. Lindén, M., Gustafsson, L. & Pärt, T. Selection of fledging mass in the collared flycatcher and the great tit. *Ecology* **73,** 336–343 (1992).
11. Both, C., Visser, M. E. & Verboven, N. Density-dependent recruitment rates in great tits: the importance of being heavier. *Proc. R. Soc. Lond. B* **266,** 465–469 (1999).
12. Sorci, G. & Clobert, J. Natural selection on hatching body size and mass in two environments in the common lizard (*Lacerta vivipara*). *Evol. Ecol. Res.* **1,** 303–316 (1999).
13. Boltnev, A. I., York, A. E. & Antonelis, G. A. Northern fur seal young: interrelationships among birth size, growth, and survival. *Can. J. Zool.* **76,** 843–854 (1998).
14. Merilä, J. Genetic variation in offspring condition—an experiment. *Funct. Ecol.* **10,** 465–474 (1996).
15. Merilä, J., Kruuk, L. E. B. & Sheldon, B. C. Natural selection on the genetical component of body condition in a wild bird population. *J. Evol. Biol.* (submitted).
16. Conover, D. O. & Schultz, E. T. Phenotypic similarity and the evolutionary significance of countergradient variation. *Trends Ecol. Evol.* **10,** 248–252 (1995).
17. Visser, M. E. & Holleman, L. J. M. Warmer springs disrupt the synchrony of oak and winter moth phenology. *Proc. R. Soc. Lond. B* **268,** 289–294 (2001).
18. Gustafsson, L. Inter- and intraspecific competition for nest holes in a population of the collared flycatcher *Ficedula albicollis*. *Ibis* **130,** 11–16 (1988).
19. Doligez, B., Danchin, E., Clobert, J. & Gustafsson, L. The use of conspecific reproductive success for breeding habitat selection in a non-colonial, hole-nesting species, the collared flycatcher. *J. Anim. Ecol.* **68,** 1193–1206 (2000).
20. Alatalo, R. V. & Lundberg, A. Density-dependence in breeding success of the pied flycatcher (*Ficedula hypoleuca*). *J. Anim. Ecol.* **53,** 969–978 (1984).
21. Lewontin, R. C. Adaptation. *Sci. Am.* **239,** 212–230 (1978).
22. Gilchrist, A. S. & Partridge, L. A comparison of the genetic basis of wing size divergence in three parallel body size clines of *Drosophila melanogaster*. *Genetics* **153,** 1775–1787 (1999).
23. Sheldon, B. C., Merilä, J., Lindgren, G. & Ellegren, H. Gender and environmental sensitivity in nestling collared flycatchers. *Ecology* **79,** 1939–1948 (1998).
24. Groeneveld, E. REML VCE, a Multivariate Multi-Model Restricted Maximum Likelihood (Co)Variance Component Estimation Package, Version 3.2 User's Guide. (Institute of Animal Husbandry and Animal Behaviour, Federal Research Center of Agriculture (FAL), Mariensee, Germany, 1995). ⟨http://www.tzv.fal.de/institut/genetik/pub/eg/vce/manual/manual.html.⟩
25. Groeneveld, E., Kovac, M., Wang, T. L. & Fernando, R. L. Computing algorithms in a general purpose BLUP package for multivariate prediction and estimation. *Arch. Anim. Breed.* **15,** 399–412 (1992).
26. Meyer, K. Restricted maximum-likelihood to estimate variance components for animal models with several random effects using a derivative-free algorithm. *Genet. Selection Evol.* **21,** 317–340 (1989).
27. Blair, H. T. & Pollak, E. J. Estimation of genetic trend in a selected population with and without the use of a control population. *J. Anim. Sci.* **58,** 878–886 (1984).
28. Southwood, O. I. & Kennedy, B. W. Genetic and environmental trends for litter size in swine. *J. Anim. Sci.* **69,** 3177–3182 (1991).
29. Merilä, J., Sheldon, B. C. & Ellegren, H. Antagonistic natural selection revealed by molecular sex identification of nestling collared flycatchers. *Mol. Ecol.* **6,** 1167–1175 (1997).
30. Genstat, 1998. Genstat 5, Release 4.1 (Lawes Agricultural Trust, IACR, Rothamsted, 1998).

Acknowledgements

We thank I. P. F. Owens, A. J. van Noordwijk, B. Walsh and D. A. Roff for comments on the manuscript, M. Visser for data on caterpillars and oaks, and the numerous people who have helped in collecting the data in the course of the study, in particular L. Gustafsson. Our research was supported by the Swedish Natural Science Research Council, the Nordic Academy for the Advanced Study (J.M.) and by Royal Society University Research Fellowships to B.C.S. and L.E.B.K.

Correspondence and requests for materials should be addressed to J.M. (e-mail: juha.merila@ebc.uu.se).

Cortical remodelling induced by activity of ventral tegmental dopamine neurons

Shaowen Bao, Vincent T. Chan & Michael M. Merzenich

Keck Center for Integrative Neuroscience, University of California, San Francisco, California 94143, USA

Representations of sensory stimuli in the cerebral cortex can undergo progressive remodelling according to the behavioural importance of the stimuli[1,2]. The cortex receives widespread projections from dopamine neurons in the ventral tegmental area (VTA)[3–5], which are activated by new stimuli or unpredicted rewards[6,7], and are believed to provide a reinforcement signal for such learning-related cortical reorganization[8]. In the primary auditory cortex (AI) dopamine release has been observed during auditory learning that remodels the sound-frequency representations[9,10]. Furthermore, dopamine modulates long-term potentiation[11,12], a putative cellular mechanism underlying plasticity[13]. Here we show that stimulating the VTA together with an auditory stimulus of a particular tone increases the cortical area and selectivity of the neural responses to that sound stimulus in AI. Conversely, the AI representations of nearby sound frequencies are selectively decreased. Strong, sharply tuned responses to the paired tones also emerge in a second cortical area, whereas the same stimuli evoke only poor or non-selective responses in this second cortical field in naïve animals. In addition, we found that strong long-range coherence of neuronal discharge emerges between AI and this secondary auditory cortical area.

In our first experiment seven rats underwent twenty 2-h daily sessions in which 9-kHz pulsed tones were paired with electrical microstimulation of the VTA (VTA/tone-paired animals; see Methods). Tone pulses preceded VTA stimulation by either 925 ($n = 3$) or 500 ms ($n = 4$). The auditory cortex was mapped in detail 24 h after the last pairing session. Because no difference was observed between the auditory cortex in animals with 925 ms and 500 ms inter-stimulus pairing intervals, data from all seven animals were pooled. Compared with naïve controls paired animals had a larger physiologically defined auditory cortex (Fig.1a, b; naïve: $1.24 \pm 0.09\,mm^2$; paired: $1.54 \pm 0.11\,mm^2$, $P < 0.05$; see Methods). In addition, a larger part of the tone-responsive auditory cortex represented the paired (9 kHz) stimulus frequency (in a range of ± 0.3 octave; $P < 0.005$). Representations of nearby frequencies (best representing 0.6 octave frequency ranges centred at 5.9 kHz and 13.6 kHz) were reduced ($P < 0.001$; Fig.2a, b).

Representations of more spectrally distant frequencies were unaltered.

These positive and negative frequency-specific representational changes resulted in emergent sharp transitions in best frequency maps (Fig. 1b, indicated by the arrows; also see Figs 1e, f and 2a). Pairing procedures did not change response properties such as latency or the number of spikes evoked by tone presentation ($P > 0.1$ for both measures; see Methods for details). On the other hand, response bandwidths at 10 and 30 dB above threshold were reduced for neurons with best frequencies near 9 kHz ($P < 0.01$; see Fig. 2c), that is, there was an increase in spectral selectivity induced by pairing of tone pulses and VTA microstimulation. Furthermore, more neurons in experimental animals exhibited non-monotonic rate–level functions in VTA/tone-paired animals ($P < 0.005$; see Figs 1f and 2d). These non-monotonic neurons may provide a basis for intensity selectivity, and may reflect another dimension of plastic remodelling that was selective for the constant-loudness paired tonal stimuli.

To ensure that effects were attributable to the activation of dopamine neurons in the VTA (or in VTA targets), three animals received systemic SCH-23390 and eticlopride (D1- and D2-type receptor antagonists) 30 min before pairing 9-kHz pulsed tones with VTA stimulation. After 20 pairing sessions identical to those used in other experimental animals the auditory cortices of these animals were indistinguishable from those of naïve controls. Neither the sizes of auditory cortex nor the percentages of the cortical areas representing the 9-kHz stimulus frequency differed between dopamine receptor antagonist and naïve rat groups (size: 1.23 ± 0.11 mm^2, $P > 0.5$ antagonist versus naïve, $P < 0.05$ antagonist versus paired, $P < 0.05$ all three groups; percentage of 9-kHz representation: $23.4 \pm 4.1\%$ for naïve group, $18.1 \pm 1.9\%$ for antagonist group, $P > 0.1$; data not shown). Dopamine neuron activity seemed to be required for the induction of cortical reorganization resulting from pairing VTA and tonal stimulation. To control for tonal exposure and VTA stimulation effects four rats were presented with 9-kHz pulsed tones and two rats received VTA stimulation for 20 sessions. No significant changes in cortical maps or receptive fields were observed in these animals (analysis of variance on total tone-responsive area, $P > 0.5$; on per cent cortex with best frequency in each frequency band, $P > 0.1$; see Supplementary Information).

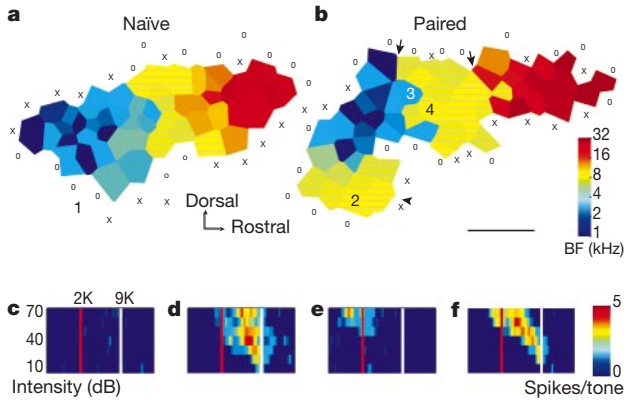

Figure 1 Representative cortical tonotopic best frequency maps and frequency-intensity receptive fields. **a**, **b**, Cortical maps from a naïve (**a**) and a VTA/tone-paired animal (**b**) (9-kHz pulsed tone). Hatched areas have best frequencies (BF) within 0.3 octaves of 9 kHz. Scale bar, 500 μm. 0, unresponsive site; X, non-AI site. The tone-responsive auditory cortex of the paired animal consists of two separate zones: AI and a ventroposterior field (arrowhead). In AI, the representation of 9 kHz was expanded while representations of adjacent frequencies were reduced, creating sharp best-frequency transitional boundaries (arrows). **c**–**f**, Receptive fields recorded from sites marked 1–4 in the two representative maps.

In reorganized maps from VTA/tone-paired animals two cortical zones developed an exaggerated response to the tonal stimulus: an AI zone with best frequencies organized in a posterior–anterior direction, and a ventroposterior field responding almost exclusively to the paired stimulus frequency (Fig. 1b, indicated by an arrowhead). In paired animals, neurons in this ventroposterior field and in AI could not be easily physiologically distinguished from each other. The fact that the ventroposterior field did not conform to the posterior–anterior-oriented rising best frequency gradient—a defining feature of the rat AI (ref. 14)—indicates that it is probably not part of AI itself. This ventroposterior zone was poorly responsive to tonal stimuli and non-selective for tone frequency in naïve animals. It becomes sharply and almost exclusively tuned to the paired stimulus frequency in VTA-stimulated animals. The position of the ventroposterior zone indicates that it is Zilles' area TE2 (ref. 15), a multimodal association area[15,16]. Dense dopamine-mediated innervation has been recorded in this region[7,8].

We separately documented the pairing-induced changes within these two remodelled tone-responsive auditory cortex zones, defining the borders between the presumptive AI and ventroposterior field by the lines of greatest best frequency transition. By that analysis, the size of AI alone was not significantly changed by the VTA/tone-pairing (naïve: 1.24 ± 0.09 mm^2; paired: 1.21 ± 0.08 mm^2, $P > 0.5$; data not shown). On the other hand, the 9-kHz representational zone in AI increased from $23.4 \pm 4.1\%$ of AI in naïve animals to $33.4 \pm 1.8\%$ in VTA/tone-paired animals ($P < 0.05$). Again, adjacent 5.9- and 13.6-kHz representations were reduced ($P < 0.05$).

The functional characteristics of a cortical neuron are defined not only by its selectivity to input parameters but also by its interactions with other neurons within cooperative neuronal ensembles. One simple measure of these interactions is the degree of synchronization of neuronal activity[17]. We analysed correlation of spontaneous multiunit activity in naïve ($n = 4$) and VTA/tone-paired rats ($n = 3$). In naïve animals correlation of discharges was higher for pairs of neurons in AI than for pairs in the surrounding belt region (including the ventroposterior field) or between AI and the belt

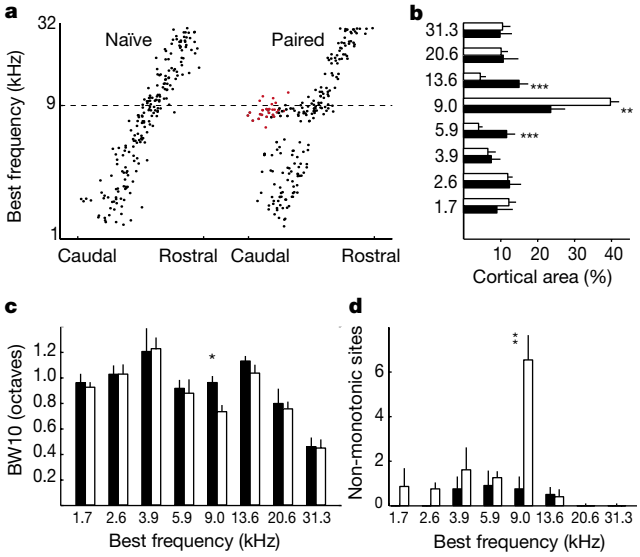

Figure 2 Reorganization of the auditory cortex by VTA microstimulation paired with a 9-kHz pulsed tone. **a**, Distribution of best frequency along the anterior–posterior axis of the auditory cortex. Points corresponding to the sites in the ventorposterior field are indicated in red ($n = 4$ for each group). **b**, Per cent of the auditory cortex that was tuned to each frequency. Black bar, naïve; white bar, paired; bin size, 0.6 octave. **c**, Response bandwidth at 10 dB (BW10) above threshold. **d**, Number of penetrations with non-monotonic rate–level function. For **b**–**d** $n = 6$ for the naïve group and $n = 7$ for the paired group. Asterisk, $P < 0.01$; double asterisk, $P < 0.005$; triple asterisk, $P < 0.001$.

region (collectively called non-AI pairs; data not shown). In general, correlation strengths decreased as a regular function of cortical distance for both AI and non-AI pairs. VTA/tone-pairing did not change the correlation–distance function of AI pairs, but resulted in a strong increase in the correlation strengths of neurons within the ventroposterior field and between the ventroposterior field and AI (Fig. 3a, b). In naïve animals discharge correlation in periods of spontaneous activity for VP–AI pairs was not different from that of other non-AI pairs separated by equivalent cross-cortical distances. However, in experimental animals VP–AI pairs showed much greater spontaneous activity correlation than did other non-AI pairs. This effect was specific for the cortical zones with altered plasticity—only activity from the AI area that represented the paired stimulus frequency (9-kHz AI) became highly correlated with activity from the emergent 9-kHz-representing ventroposterior zone ($P < 0.001$, between red dots and black circles in Fig. 3a, with distance ranging from 700 to 1,600 μm). Notably, these two regions were commonly more than 1 mm apart and were always separated by areas in which discharges were not measurably correlated with discharges of neurons within the ventroposterior zone (Fig. 3b). More AI pairs (83 and 80% for naïve and paired rats, respectively) showed time lags of near zero (< 3ms), as compared with non-AI pairs (59 and 51% for naïve and paired animals, respectively, excluding VP/9-kHz-AI pairs, Kolmogorov–Smirnov test; $P < 0.05$). The time lag distribution of the VP/9-kHz-AI pairs was comparable to that for AI pairs (82% near-zero time lag, Kolmogorov–Smirnov test; $P > 0.1$).

These results indicate that VTA dopamine neuron activity paired with sensory stimulation can induce long-range, cross-area-synchronization of neuronal activity. They suggest that the VTA dopamine system may mediate the learning-based grouping of cortical neurons into distributed functional neuronal assemblies[17].

Dopamine is believed to be involved in reinforcement learning[4–6] in which a reward is associated with preceding but not following events[5]. We tested whether a similar temporal specificity can be obtained for this tone/VTA-pairing-induced cortical plasticity. In three rats VTA activity was preceded by a 4-kHz pulsed tone and followed by a 9-kHz pulsed tone. After 20 days of pairing, the cortical representation of 4 kHz was significantly expanded ($P < 0.0005$). The representations of adjacent 9-kHz frequencies were significantly reduced ($P < 0.05$; see Fig. 4). In addition, the ventroposterior field became well tuned to 4 kHz but not 9 kHz tones (Fig. 4). Thus, cortical reorganization enabled by VTA activity seemed to selectively enhance the saliency of the stimuli that consistently preceded and, therefore, predicted the VTA activity, and also to selectively attenuate the saliency of a stimulus that immediately followed VTA activity.

The specific mechanisms by which the dopamine system modulates reorganization of the cortex are unclear. The dense distribution of dopamine receptors in the superficial and deep layers of the cortex suggests that the dopamine system may be involved in the modulation of strengthening and weakening corticocortical connections[7–9]. This is consistent with our findings that dopamine activity paired with sensory stimuli can enhance long-range, in-phase neuronal synchronization, which is mediated by corticocortical connections[18,19]. Cooperative interactions between the ventroposterior field and the AI plausibly contribute to the receptive field and map changes recorded in these two zones.

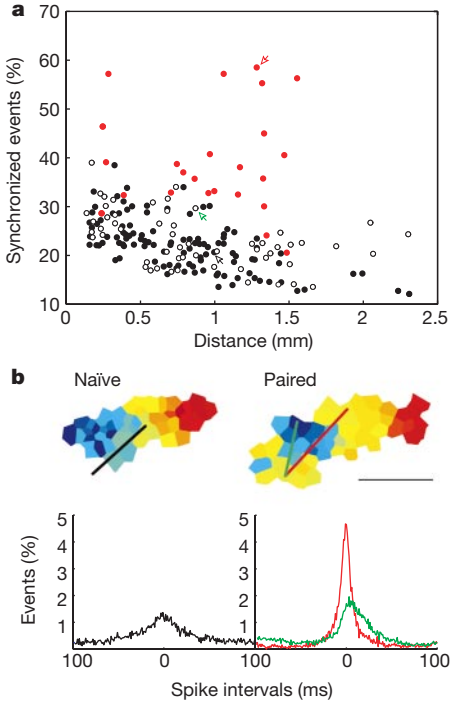

Figure 3 VTA/tone-pairing increases neuronal synchrony between the ventroposterior region and the 9-kHz-representing AI area. **a**, Synchronization–distance functions involving at least one penetration outside AI. Data from naïve animals are plotted as black dots. Data from VTA-stimulated animals were separated into two groups: pairs within the ventroposterior field and pairs between the ventroposterior field and the 9-kHz-AI area are plotted as red dots; the rest are plotted as open circles. **b**, Examples of correlograms. Black, VP/AI pair from a naïve animal; red, VP/9-kHz-AI pair from a VTA-stimulated animal; green, VP/non-9-kHz-AI pairs from the same VTA-stimulated animal. The locations of the recording sites in the best frequency maps are shown in the insets and the corresponding data points are indicated in **a** with arrows. Scale bar, 1 mm.

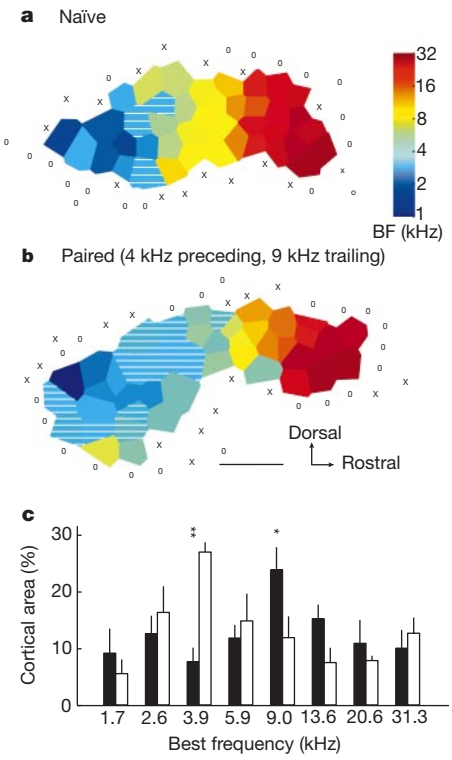

Figure 4 VTA stimulation effects are temporally asymmetrical. **a**, Representative cortical best frequency (BF) map from a naïve animal. **b**, Cortical map of an animal that received VTA stimulation paired with two pulsed tones. The first 4-kHz tone preceded the VTA stimulation by 500 ms; the second 9-kHz tone followed the VTA stimulation 500 ms later. Neurons recorded in hatched areas had best frequencies within 0.3 octave of 4 kHz. Scale bar, 500 μm. 0, unresponsive site; X, non-AI site. **c**, Per cent of auditory cortex that was tuned to each frequency ($n = 6$ for naïve group and $n = 3$ for paired group). Asterisk, $P < 0.05$; double asterisk, $P < 0.0005$.

Table 1 Characteristics of auditory cortical plasticity

	VTA	Nucleus basalis*
Size of functional auditory cortex	Increased	Increased
Size of functional AI	No change	Increased
Stimulus frequency representation	Increased	Increased
Adjacent frequency representation	Decreased	Increased
Spectral selectivity	Increased	No change
Non-monotonic responses	Increased	No change
Frequency specificity of the effects	Sharper	Broader
Tuning of secondary auditory cortex	Yes	No
Temporal asymmetry of the effects	Yes	No
Modulation of stimulus-following rate	Undetermined	Yes
Cross-area synchronization	Yes	Does not apply

Auditory cortical plasticity was induced by pairing brain microstimulation with a tonal stimulus.
*Values of nucleus basalis are from refs 14, 22 and 23.

It should be emphasized that our dopamine receptor-blocking controls do not elucidate specific mechanisms accounting for cortically induced change. VTA neurons project complexly to other neuromodulatory nuclei[20], and indirect plasticity modulation effects may also have occurred. One of those indirect targets of the VTA is the nucleus basalis[20,21]. Studies have already shown that powerful plastic changes can be induced in the AI in adult rats by pairing tonal stimulation with nucleus basalis stimulation following an experimental model that is similar to that applied in our study. On the other hand, changes recorded in VTA/tone-paired rats was different, in many respects, from the plasticity induced by nucleus basalis stimulation/tone pairing[14,22,23] (see Table 1). The marked differences between VTA and nucleus basalis plasticity modulation show that changes recorded with VTA stimulation are not dominated by, and probably not substantially attributable to, indirectly engaged acetylcholine-mediated neuromodulatory inputs from the nucleus basalis. It should also be noted that VTA stimulation differs from natural activation of dopamine neurons in that it does not reflect an error in reward prediction.

The cortex is thought to be hierarchically organized, with progressively more complex information processing contributed by 'higher-level' cortical areas[24]. Most studies have focused on plasticity in primary sensory and motor cortices and on its involvement in shaping sensory processing or motor control capabilities[11,13,14,22,23,25–29]. In the present study, as has been indicated in earlier classical conditioning experiments[30], we have shown that a secondary auditory cortical zone is also subject to large-scale plasticity-induced reorganization. The 'association' cortex that has been altered by VTA/tone-pairing in the current studies has been described as diversely connected with sensory, limbic and paralimbic cortical areas, suggesting that it is involved in cross-modal sensory integration, association of emotion with sensory stimuli, and learning[16]. These and other studies strongly indicate that dopamine-enabled reorganization of this prospective association cortical area may have an important role in the progressive development of those cortical functions.

Our results directly demonstrate that ventral tegmental dopamine-mediated activity enables the reorganization of the cerebral cortex. The critical roles of central neuromodulatory systems in maintaining and shaping cerebral cortex network, and thereby cortical function, are just beginning to be understood. Further studies should now rapidly advance our understanding of the specific roles of different neuromodulatory systems as critical agents contributing powerfully to the progressive development of the functional capacities of the brain. □

Methods

Preparation

Platinum bipolar-stimulating electrodes were stereotaxically implanted within the right VTA (4.5 mm posterior, 0.7 mm lateral and 8.5 mm ventral to Bregma) in female rats anaesthetized with barbiturate (300 g), using techniques approved under University of California, San Francisco Animal Care Facility protocols. After a two-week recovery period rats were placed in an operant conditioning chamber and were allowed to bar press for brief VTA microstimulation (10 biphasic pulses of 0.1-ms duration at 100 Hz). The minimal current levels that reinforced consistent bar presses at least once every 2 s were determined as the electrical stimulus threshold (100–200 μA). Subsequent pairing of auditory stimuli with VTA stimulation took place in a sound-attenuation chamber. One group of seven rats was presented with paired 9-kHz pulsed tone (six 25-ms tone pips with 5-ms on/off ramp delivered at a rate of 10 pips s^{-1}, 55 dB peak intensity) and VTA electrical microstimulation (10 biphasic pulses of 0.1-ms duration at 100 Hz, started 500 ms after tone onset). The intervals between successive pairing trials were pseudorandom in the range from 12 to 28 s. Three animals in this group were also given systemic D1 and D2 receptor antagonists (SCH-23390 and eticlopride, 0.1 and 0.3 mg kg, respectively, administered intraperitoneally 30 min before each daily pairing session. A second group of three animals underwent the same pairing procedure as the first group, except that the VTA stimulation trailed the pulsed tone by 925 ms. A third group of three animals received pairings of VTA stimulation with pulsed tones of different frequencies: a 4-kHz pulsed tone preceded the VTA stimulation and a 9-kHz pulsed tone followed it. The onset intervals between each of the tones and the onset of the VTA stimulation were both 500 ms. To control for stimulus-induced changes in the auditory cortex four animals were presented with 9-kHz pulsed tones and two animals with VTA stimulation alone.

Electrophysiology

In six naïve rats and 24 h after the last stimulation session in the experimental and control rats, animals were anaesthetized with sodium pentobarbital, the right auditory cortex surgically exposed, and neuronal responses recorded with parylene-coated tungsten microelectrodes. We chose penetration sites to evenly sample from the auditory cortical zone while avoiding blood vessels. At every penetration site the recording microelectrode was lowered orthogonal to the surface 470–550 μm in depth (layers 4/5), where vigorous driven responses were recorded. We collected the evoked spikes of a neuron or a small cluster of 2–5 neurons at each site. Frequency/intensity response areas were reconstructed in detail by presenting 60 pure-tone frequencies (0.5–30 kHz, 25-ms duration, 5-ms ramps) at each of eight sound intensities to the contralateral ear at a rate of two stimuli per s using a calibrated sound-delivering system. The tuning curve characterization was made with a 'blind' procedure. A best frequency (recorded objectively) was defined as the frequency that evoked a neuronal response at the lowest stimulus intensity. To generate best frequency maps, points on the cortex were assigned the best frequencies of nearest penetrations through Voronoi tessellation[14]. The boundaries of the map were functionally determined using sites that did not have a well defined, tone-evoked receptive field. The response latency was defined as the time from stimulus onset to the earliest response for any of the eight intensities of the five frequencies that were nearest the best frequency. Response amplitude was defined as the average number of spikes per tone for five frequencies nearest the best frequency at 70 dB. Response latencies and amplitudes were analysed only for sites with a well defined receptive field.

To analyse neuronal discharge correlation, spontaneous activity was simultaneously recorded from three to four sites for 30 periods of non-stimulus spontaneous activity that were 2 s in duration. For each recording pair a cross-correlogram (a histogram of between-site spike intervals) was constructed from −100 ms to 100 ms. An interval less than 10 ms was considered as a synchronized event. The degree of synchronization was assessed using per cent of synchronized events. Time lag was defined as the spike interval at the peak of the correlogram. Unless otherwise specified in the text statistical significance was assessed using a two-tailed *t*-test. Data are presented as mean ± s.e.m. On completion of the experiment electrolytic lesions were made through the stimulating electrodes and the placement of the stimulating electrodes in the VTA was verified with histological examinations.

Received 28 March; accepted 2 May 2001.

1. Buonomano, D. V. & Merzenich, M. M. Cortical plasticity: from synapses to maps. *Annu. Rev. Neurosci.* **21,** 149–186 (1998).
2. Sanes, J. N. & Donoghue, J. P. Plasticity and primary motor cortex. *Annu. Rev. Neurosci.* **23,** 393–415 (2000).
3. Foote, S. L. & Morrison, J. H. Extrathalamic modulation of cortical function. *Annu. Rev. Neurosci.* **10,** 67–95 (1987).
4. Goldsmith, S. K. & Joyce, J. N. Dopamine D2 receptors are organized in bands in normal human temporal cortex. *Neurosci.* **74,** 435–451 (1996).
5. Lidow, M. S., Goldman-Rakic, P. S., Gallager, D. W. & Rakic, P. Distribution of dopaminergic receptors in the primate cerebral cortex: quantitative autoradiographic analysis using (^{3}H)raclopride, (^{3}H)spiperone and (^{3}H)SCH23390. *Neruoscience* **40,** 657–671 (1991).
6. Hollerman, J. R. & Schultz, W. Dopamine neurons report an error in the temporal prediction of reward during learning. *Nature Neurosci.* **1,** 304–309 (1998).
7. Schultz, W. & Dickinson, A. Neuronal coding of prediction errors. *Annu. Rev. Neurosci.* **23,** 473–500 (2000).
8. Montague, P. R., Dayan, P. & Sejnowski, T. J. A framework for mesencephalic dopamine systems based on predictive Hebbian learning. *J. Neurosci.* **16,** 1936–1947 (1996).
9. Stark, H. & Scheich, H. Dopaminergic and serotonergic neurotransmission systems are differentially involved in auditory cortex learning: a long-term microdialysis study of metabolites. *J. Neurochem.* **68,** 691–697 (1997).
10. Bakin, J. S., South, D. A. & Weinberger, N. M. Induction of receptive field plasticity in the auditory cortex of the guinea pig during instrumental avoidance conditioning. *Behav. Neurosci.* **110,** 905–913 (1996).
11. Gurden, H., Takita, M. & Jay, T. M. Essential role of D1 but not D2 receptors in the NMDA receptor-dependent long-term potentiation at hippocampal-prefrontal cortex synapses *in vivo*. *J. Neurosci.* **20,** RC106, 1–5 (2000)..
12. Otmakhova, N. A. & Lisman, J. E. D1/D5 dopamine receptors inhibit depotentiation at CA1 synapses via cAMP-dependent mechanism. *J. Neurosci.* **18,** 1270–1279 (1998).

13. Rioult-Pedotti, M.-S., Friedman, D. & Donoghue, J. P. Learning-induced LTP in neocortex. *Science* **290,** 533–536 (2000).
14. Kilgard, M. P. & Merzenich, M. M. Cortical map reorganization enabled by nucleus basalis activity. *Science* **279,** 1714–1718 (1998).
15. Zilles, K. in *The Cerebral Cortex of the Rat* (eds Kolb, B. & Tees, R. C.) 77–112 (MIT, Cambridge, Massachusetts, 1990).
16. Pandya, D. N. & Seltzer, B. Association areas of the cerebral cortex. *Trends Neurosci.* **5,** 386–390 (1982).
17. Singer, W. Neuronal synchrony: a versatile code for the definition of relations? *Neuron* **24,** 49–65 (1999).
18. Engel, A. K., König, P., Kreiter, A. K. & Singer, W. Interhemispheric synchronization of oscillatory neuronal responses in cat visual cortex. *Science* **252,** 1177–1179 (1991).
19. Traub, R. D., Whittington, M. A., Stanford, I. M. & Jefferys, J. G. A mechanism for generation of long-range synchronous fast oscillations in the cortex. *Nature* **383,** 621–624 (1996).
20. Oades, R. D. & Halliday, G. M. Ventral tegmental (A10) system: neurobiology. 1. Anatomy and connectivity. *Brain Res.* **434,** 117–165 (1987).
21. Haring, J. H. & Wang, R. Y. The identification of some sources of afferent input to the rat nucleus basalis magnocellularis by retrograde transport of horseradish peroxidase. *Brain Res.* **366,** 152–158 (1986).
22. Kilgard, M. P. & Merzenich, M. M. Plasticity of temporal information processing in the primary auditory cortex. *Nature Neursci.* **1,** 727–731 (1998).
23. Bakin, J. S. & Weinberger, N. M. Induction of a physiological memory in the cerebral cortex by stimulation of the nucleus basalis. *Proc. Natl Acad. Sci. USA* **93,** 11219–11224 (1996).
24. Van Essen, D. C., Anderson, C. H. & Felleman, D. J. Information processing in the primate visual system: an integrated systems perspective. *Science* **255,** 419–423 (1992).
25. Tremblay, N., Warren, R. A. & Dykes, R. W. Electrophysiological studies of acetylcholine and the role of the basal forebrain in the somatosensory cortex of the cat. II. Cortical neurons excited by somatic stimuli. *J. Neurophysiol.* **64,** 1212–1222 (1990).
26. Sachdev, R. N., Lu, S. M., Wiley, R. G. & Ebner, F. F. Role of the basal forebrain cholinergic projection in somatosensory cortical plasticity. *J. Neurophysiol.* **79,** 3216–3228 (1998).
27. Jenkins, W. M., Merzenich, M. M., Ochs, M. T., Allard, T. & Guic-Robles, E. Functional reorganization of primary somatosensory cortex in adult owl monkeys after behaviorally controlled tactile stimulation. *J. Neurophysiol.* **63,** 82–104 (1990).
28. Recanzone, G. H., Schreiner, C. E. & Merzenich, M. M. Plasticity in the frequency representation of primary auditory cortex following discrimination training in adult owl monkeys. *J. Neurosci.* **13,** 87–103 (1993).
29. Nudo, R. J., Wise, B. M., SiFuentes, F. & Milliken, G. W. Neural substrates for the effects of rehabilitative training on motor recovery after ischemic infarct. *Science* **272,** 1791–1794 (1996).
30. Diamond, D. M. & Weinberger, N. M. Classical conditioning rapidly induces specific changes in frequency receptive fields of single neurons in secondary and ventral ectosylvian auditory cortical fields. *Brain Res.* **372,** 357–360 (1986).

Supplementary information is available on *Nature*'s World-Wide Web site (http://www.nature.com) or as paper copy from the London editorial office of *Nature*.

Acknowledgements

We thank D. Blake for many informative suggestions; L. I. Zhang and F. Strata for discussions; and C. Garabedian and T. Moallem for comments on the manuscript. This work was supported by an NIH grant, the Coleman Fund, the Mental Insight Foundation, and Hearing Research.

Correspondence and requests for materials should be addressed to M.M.M. (e-mail: merz@phy.ucsf.edu).

The glyoxylate cycle is required for fungal virulence

Michael C. Lorenz & Gerald R. Fink

Whitehead Institute for Biomedical Research, Nine Cambridge Center, Cambridge, Massachusetts 02142, USA

***Candida albicans*, a normal component of the mammalian gastrointestinal flora, is responsible for most fungal infections in immunosuppressed patients. *Candida* is normally phagocytosed by macrophages and neutrophils, which secrete cytokines and induce hyphal development in this fungus[1,2]. Neutropenic patients, deficient in these immune cells, are particularly susceptible to systemic candidiasis[3,4]. Here we use genome-wide expression profiles of the related yeast *Saccharomyces cerevisiae* to obtain a signature of the events that take place in the fungus on ingestion by a mammalian macrophage. Live *S. cerevisiae* cells isolated from the phagolysosome are induced for genes of the glyoxylate cycle, a metabolic pathway that permits the use of two-carbon compounds as carbon sources. In *C. albicans*, phagocytosis also upregulates the principal enzymes of the glyoxylate cycle, isocitrate lyase (ICL1) and malate synthase (MLS1). *Candida albicans* mutants lacking *ICL1* are markedly less virulent in mice than the wild type. These findings in fungi, in conjunction with reports that isocitrate lyase is both upregulated and required for the virulence of *Mycobacterium tuberculosis*[5,6], demonstrate the wide-ranging significance of the glyoxylate cycle in microbial pathogenesis.**

Systematic studies of host–pathogen interactions have been hampered by the lack of genetic tools in *C. albicans*. For this reason the related but non-pathogenic yeast *S. cerevisiae* is often used to uncover relevant genes. *In vitro*, cultured mammalian macrophages readily ingest both *S. cerevisiae* and *C. albicans* cells. A population of *S. cerevisiae* highly enriched for phagocytosed cells was isolated and subjected to whole-genome microarray analysis using oligonucleotide-based arrays (Affymetrix). Three hours after initiating the co-culture, most of the phagocytosed cells were alive (averaging 67% alive, as assayed by methylene blue staining); transcriptional profiling of these cells reveals the response of fungal cells to phagocytosis.

Eleven of the fifteen most highly induced *S. cerevisiae* genes after phagocytosis (Table 1) encode proteins related to the glyoxylate cycle, through which two-carbon compounds are assimilated into the tricarboxylic acid (TCA) cycle (see Fig. 1). Three of the five glyoxylate cycle enzymes are on this list (isocitrate lyase, ICL1; malate synthase, MLS1; and malate dehydrogenase, MDH2), and a fourth (citrate synthase, CIT2) is also strongly induced (4.9-fold, ranking 24th). Furthermore, several genes functionally related to the glyoxylate cycle are induced, including acetyl coenzyme A (acetyl-CoA) synthase (ACS1); YDR384c, a homologue of the *Yarrowia lipolytica* glyoxylate pathway regulator (GPR1; refs 7, 8); several transporters and acetyltransferases, which are used to traffic intermediates of the glyoxylate cycle and fatty-acid degradation between organelles (CRC1, ACR1, YAT1 and YER024w); and fructose-1,6-bisphosphatase (FBP1). FBP1 is a central regulatory point in gluconeogenesis[9]—the production of glucose is the principal function of the glyoxylate cycle. Induction of the glyoxylate cycle indicates that nutrient acquisition and use is the primary focus of yeast cells upon phagocytosis, presumably because the phagolysosome is poor in complex carbon compounds (see Fig. 1).

Although the glyoxylate cycle and TCA share common reactions, it is only the isozymes specialized for the glyoxylate cycle that are induced (Fig. 1). The cytosolic isozyme of MDH2, which preferentially functions in the glyoxylate cycle[10], is induced 15.6-fold. By contrast, the mitochondrial (MDH1) and peroxisomal (MDH3) forms are not induced. Out of the three citrate synthase isoforms only the glyoxylate cycle-specific CIT2 is induced. In control array experiments expression of glyoxylate cycle enzymes were not changed significantly in response to conditioned media, oxidative stress, or contact with heat-killed macrophages (see Methods). Thus, phagocytosis specifically upregulates the glyoxylate cycle and its accessory proteins. This metabolic response takes precedence over any conventional stress response, suggesting that nutrient deprivation is the primary 'stress' that confronts these cells.

We cloned the *C. albicans* genes for isocitrate lyase (*ICL1*) and malate synthase (*MLS1*), the only enzymes whose activity is both specific and limited to the glyoxylate cycle. Both genes share significant homology with proteins from fungi, plants and bacteria but, notably, not mammals, which do not have the glyoxylate cycle. Northern analysis of RNA from both *S. cerevisiae* and *C. albicans* cells grown in the presence of macrophages shows that in both organisms the *ICL1* or *MLS1* (Fig. 2a, b) genes are significantly induced by macrophage contact when compared with cells grown in media alone. Thus, the induction of the glyoxylate enzymes is a